Experimental investigation of thin steel plate shear walls with different infill-to-boundary frame connections

Cüneyt vatansever[1]*, Nesrin yardımcı[2]

[1]*Department of Civil Engineering, Faculty of Civil Engineering, Istanbul Technical University, Istanbul, Turkey*
[2]*Department of Civil Engineering, Faculty of Engineering, Yeditepe University, Istanbul, Turkey*

Abstract. To make direct comparisons regarding the cyclic behavior of thin steel plate shear walls (TSPSWs) with different infill-to-boundary frame connections, two TSPSWs were tested under quasi-static conditions, one having the infill plate attached to the boundary frame members on all edges and the other having the infill plate connected only to the beams. Also, the bare frame that was used in the TSPSW specimens was tested to provide data for the calibration of numerical models. The connection of infill plates to surrounding frames was achieved through the use of self-drilling screws to fish plates that were welded to the frame members. The behavior of TSPSW specimens are compared and discussed with emphasis on the characteristics important in seismic response, including the initial stiffness, ultimate strength and deformation modes observed during the tests. It is shown that TSPSW specimens achieve significant ductility and energy dissipation while the ultimate failure mode resulted from infill plate fracture at the net section of the infill plate-to-boundary frame connection after substantial infill plate yielding. Experimental results are compared to monotonic pushover predictions from computer analysis using strip models and the models are found to be capable of approximating the monotonic behavior of the TSPSW specimens.

Keywords: steel plate shear wall, semi-rigid connection, self-drilling screw, cyclic loading, initial stiffness, ultimate strength, energy dissipation.

1. Introduction

To date, several experimental and numerical researches have been conducted on thin steel plate shear walls (TSPSWs). However, investigation of TSPSWs having the infill plate connected only to the beams of the boundary frame is limited in scope. Numerical research has been conducted (Xue and Lu, 1994) and also an experimental investigation (Choi and Park, 2009) has been performed and demonstrated that this type of TSPSWs had excellent deformation and load-carrying capacity, initial stiffness and energy dissipation capacity. Furthermore, such systems may have considerable benefits in terms of ease of construction and in reducing the flexural demands on the boundary frame columns imposed by the infill plate. Therefore, a need exists to experimentally investigate the behavior of the TSPSWs with infill plates having such connection to the boundary frame and to study the strength, stiffness and ductility of the system.

The general behavior of steel plate shear walls with thin infill plates is characterized by infill plate

---

* Corresponding author, PhD., E-mail: cuneyt.vatansever@itu.edu.tr.

buckling that occurs at low loads and the development of tension field action that provides the lateral resistance of the SPSW. The acceptance of relying on tension field action for lateral resistance has resulted in more economical SPSW designs. Further, SPSWs have been also shown to have excellent seismic performance as they are excellent ductile, have a robust resistance to degradation under cyclic loading and have a high initial stiffness.

Since the 1970s, researchers have experimentally and analytically studied the behavior of SPSWs and have shown that SPSWs can be a useful seismic load resisting system (Thorburn *et al.* 1983, Timler and Kulak 1983, Tromposch and Kulak 1987, Caccese *et al.* 1993, Elgaaly and Liu 1997, Driver *et al.* 1998, Lubel *et al.* 2000). Additionally, an experimental research program on prototype light-gauge steel plate shear walls which were designed as a seismic retrofit demonstrated that adding infill plates to steel frames achieved the goals of increased stiffness, energy dissipation capability and ductility (Berman and Bruneau 2005). The influence of the axial and flexural stiffness of the boundary frame members on the behavior of TSPSWs has been investigated (Alinia and Dastfan 2006), several studies have focused on aspects of TSPSW design and have resulted in a plastic design method (Berman and Bruneau 2003), a component-based design method considering the strength contributions of the frame and infill plates separately (Sabouri-Ghomi *et al.* 2005) and a performance-based design procedure based on a target inelastic drift and a pre-selected yield mechanism (Ghosh *et al.* 2009). In addition, a parametric study was carried out on buckling loads and tension field stress patterns of steel plate shear walls concerning buckling modes (Memarzadeh *et al.* 2010).

TSPSW systems could also be effective alternatives for the seismic retrofit of buildings (Bruneau and Bhagwagar 2002, Vian *et al.* 2009). To provide optimal performance, infill plates should be attached to the boundary frame on all edges. However, attaching each infill plate edge involves welding fish plates to the boundary frame members and then attaching the infill plates via bolts or welds. Thus, each attachment results in labor and material costs as well as construction time. Alternatively, infill plates can be connected to boundary frame beams only to provide time, labor and material savings. It is anticipated that the behavior of these kinds of systems will be different in that they will likely have reduced energy dissipation, initial stiffness and ductility than conventional TSPSWs. However, it is expected that such shortcomings can be overcome via proper design of the systems. Furthermore, due to the absence of the infill plate-to-column connections there will be no forces pulling in on the columns from the infill plates, making the system more viable in retrofit situations where the columns may not have adequate strength or stiffness to resist the pull-in forces necessary to achieve the infill plate's tensile yield strength.

Here, an experimental investigation is described that focuses on the cyclic behavior of TSPSWs with and without infill plate connections to the boundary frame columns. Three specimens are tested under quasi-static cyclic loading, including two TSPSWs and one bare boundary frame whose test results are used for the calibration of semi-rigid beam-to-column connection models that are then employed in simple models of the TSPSW. The behavior of the specimens is quantified in terms of ductility, energy dissipation, and initial stiffness. Numerical analyses of the specimens were also performed with an accepted simple model for TSPSWs. Additional information and data from this research program may be found in Vatansever (2008).

2. Design of single-story specimens and setup

Two TSPSWs, denoted SW-A-H and SW-B-H, were designed for quasi-static testing. Specimen SW-

A-H was designed with the infill plate attached to boundary frame members on all four sides while Specimen SW-B-H was designed with the infill plate connected only to the beams of the boundary frame. Additionally, a bare frame, denoted BF-H, was tested to document the behavior of the system without the infill plates. The specimens were designed at 1/3 scale due to actuator force limitations and space restrictions. Overall specimen dimensions including the bay width, *L*, story height, *H*, taken as centerline dimensions of the frame, and the infill plate thicknesses, *t*, are summarized in Table 1. As shown in the table, the specimens had thin infill plates meaning that several such infill plates may be required for a retrofit application. The resulting slenderness ratio of the infill plate (*L/t*) was 3600 for both TSPSW specimens. The boundary frame members were designed to remain elastic, resulting in HE 280 B columns and IPE 270 beams. This was done so these members could be reused after for additional tests.

Specimens SW-A-H and SW-B-H are shown in Figs. 1 and 2 respectively. Specimen BF-H is the boundary frame of the TSPSW specimens with no other differences. The boundary frame was tested to document the improvement in performance provided by the infill plates and to develop an analytical model that includes the beam-to-column connection behavior that can then be used in models of TSPSWs.

The beam-to-column connections were header plate connections that used end plates shorter than beam depth which were welded to the beam web and bolted to the column flanges by M16-10.9 bolts (16 mm diameter with a yield stress of 900 MPa and tensile stress of 1000 MPa). The use of thin infill plates in retrofit applications requires the use of unconventional fasteners for attaching them to the boundary frame. As with all infill plate connections, the goal is to develop the full tension field yield strength of plates. Here, the infill plate thickness of 0.50 mm prohibited welding or using large diameter bolts. Instead, the infill plates were attached to fish plates using self-drilling screws with a nominal

Table 1 Test specimen details

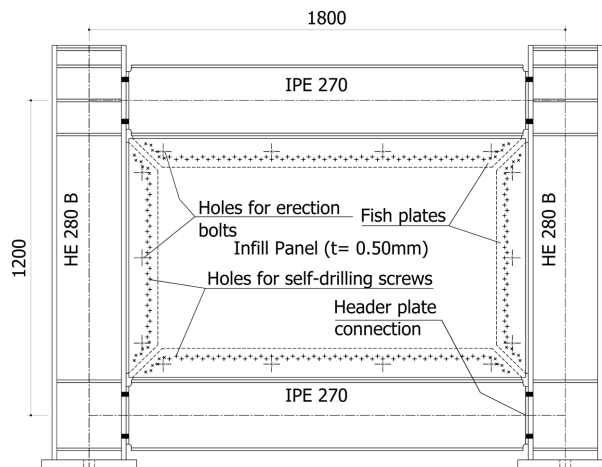| Specimen	Overall dimensions (L/H) [mm]	Nominal plate thickness (t) [mm]	Slenderness ratio (L/t)
BF-H	1800/1200	-	-
SW-A-H	1800/1200	0.50	3600
SW-B-H	1800/1200	0.50	3600

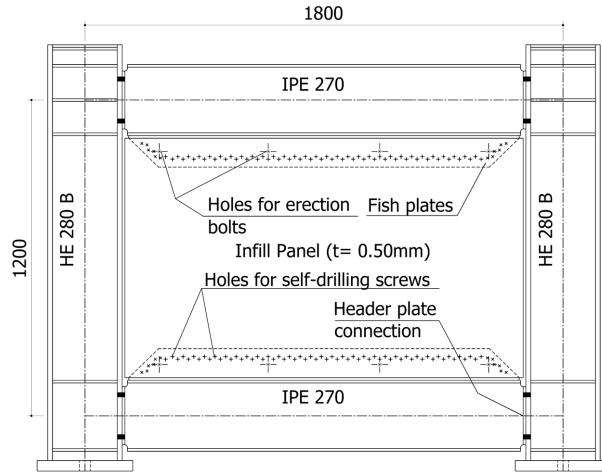Fig. 1 Details of specimen SW-A-H (Dimensions in mm).

Fig. 2 Details of specimen SW-B-H (Dimensions in mm)

diameter of 5.50 mm. The advantage of using self-drilling screws over welding is that as relatively thin infill plate is needed to use, self-drilling screws may be an alternative fastener to avoid the local deformations in the connections caused by high welding heat. Moreover, unless in bolted connections the use of self-drilling screws may not require the pre-holes for their connections before their application. The use of self-drilling screws is another unique aspect of this research as their ability to provide adequate performance in connecting the infill plate to the fish plate is investigated. The fish plates were then welded to the boundary frame members. Details of both the infill plate-to-fish plate connection and the beam-to-column are shown in Fig. 3.
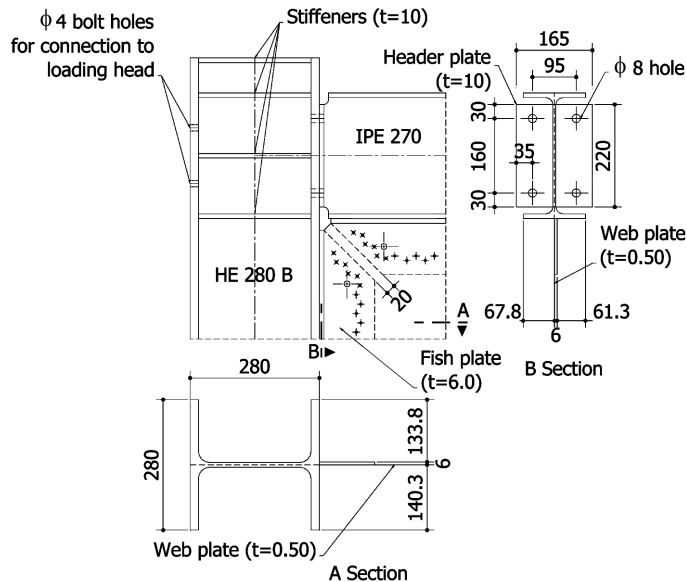

Fig. 3 Infill plate-to-boundary frame and beam-to-column connections detail (Dimensions in mm)

Two screw lines were used with a 10mm distance between them to accommodate the required number of screws. A minimum distance between two screws of three times the diameter of the screw was used as that was thought to be adequate to prevent net section fracture of the infill plate prior to achieving yield. The holes in the two lines were staggered as shown in Fig. 4. A limited number of erection bolts were included to help in properly installing the infill plates. To avoid the plate net-area fracture at the infill-to-boundary frame connections, first, infill plates are represented by a series of discrete, tension-only strips inclined in the direction of the tension field. Then, each end connection of the strips is designed in such a way that the fracture strength of the strip net section area would be greater than the yield strength of the strip gross area.

Fig. 5, is a schematic of the experimental setup and is presented to aid in the description of the design of the surrounding frames and test setup. As shown, foundation plates were fixed to a very stiff foundation slab which was connected to the reinforced concrete strong floor. Each specimen was mounted on clevises designed to interface with the foundation plates. A servo-controlled hydraulic
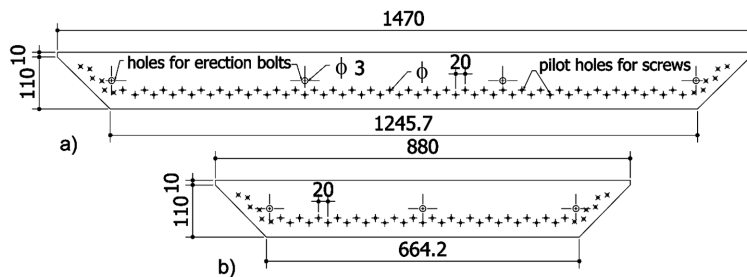

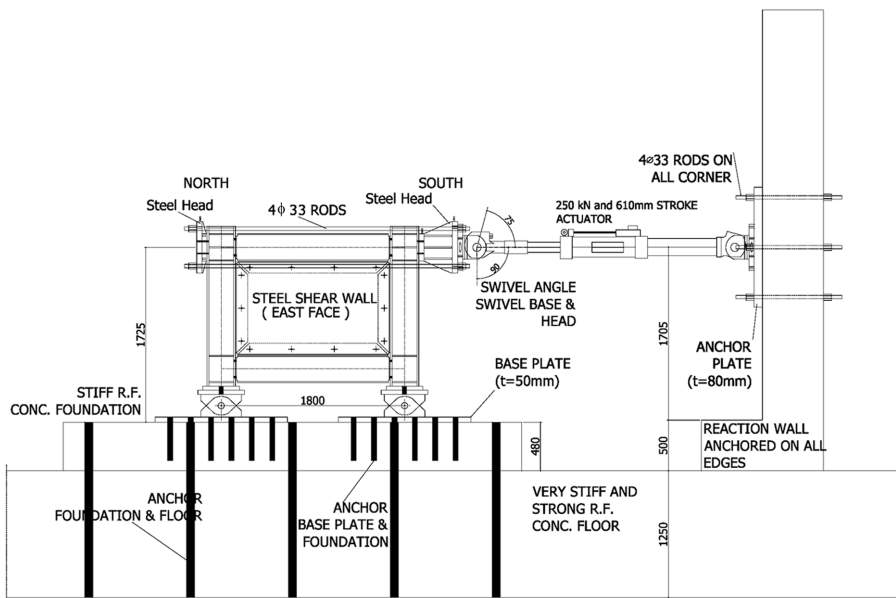Fig. 4 Details of fish plates connected to; a) beams and b) columns (Dimensions in mm)
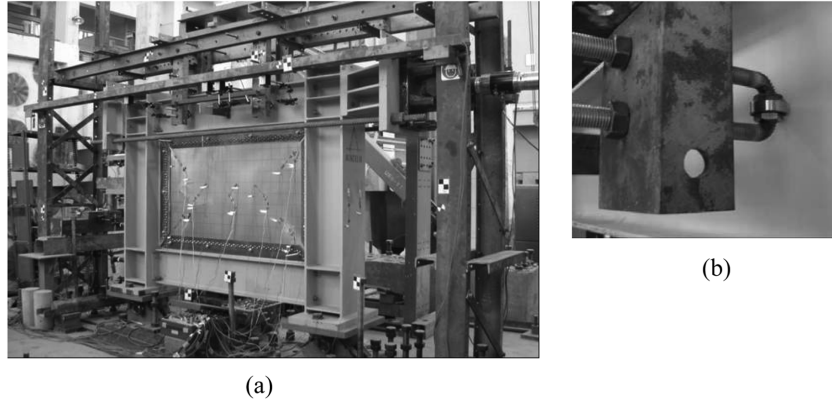

Fig. 5 Test setup (Dimensions in mm)

Fig. 6 (a) Specimen, clevises and lateral bracing system, (b) Detail of lateral bracing

actuator was mounted between the specimen and the laboratory's reinforced concrete reaction wall.

Lateral bracing was provided to the specimen through the use of steel rollers as shown in Fig. 6 that were cantilevered from frames mounted on the east and west side of the specimen and set to roll at mid-depth of the web of the specimen's upper beam.

3. Materials tests

Uniaxial tension tests of the infill plates material were conducted and the resulting stress-strain curves are shown in Figs. 7(a-b). Table 2 provides material property results for the for the header plates. In this table, elastic modulii are calculated using a linear curve fit through the appropriate test data in elastic
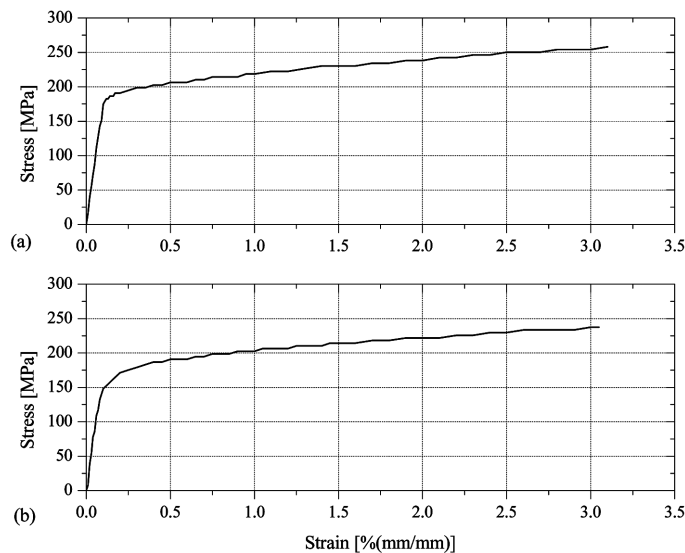

Fig. 7 Infill plate coupon test results (a) Specimen SW-A-H (b) Specimen SW-B-H

Table 2 Header plate coupon test results

Coupon mark	Width [mm]	Thickness [mm]	Elastic modulus [MPa]	Yield stress [MPa]	Ultimate stress [MPa]
Header plate					
BEP1	24.75	10	188208	301.1	425.9
BEP2	25.1	10.1	210825	301.7	421.6
BEP3	24.9	9.9	179019	302.3	423.7
Mean			192684	301.7	423.7

range. Yield stresses of 198.5 and 179.1 MPa and ultimate stresses of 333.5 and 311.9 MPa were obtained for the infill plates of SW-A-H and SW-B-H, respectively. Elastic modulii of 198515 and 194623 MPa were also obtained for the infill plate materials of SW-A-H and SW-B-H, respectively.

Material tests on the steel used for the surrounding frames and fish plates were not performed since these members were expected to remain elastic during the experiments. The material of boundary frames and fish plates was specified to be S275 (yield stress, 275 N/mm^2) and S235 (yield stress, 235 N/mm^2), respectively.

4. Modeling of the specimens

The TSPSW specimens were modeled in ABAQUS/Standard (Hibbit *et al.* HKS) using the strip model representation. These models were used to predict the global yield force and displacement of the TSPSW specimens, facilitate a comparison with experimental results, and to explore the use of the strip model for representing infill plates that are connected only to the beams. In all models, beam elements (ABAQUS element B31) were used for boundary frame members.

Additionally, all models were pinned at the column bases to replicate the test conditions. Boundary conditions preventing out-of-plane displacements were imposed at upper beam. The infill plates were represented by a series of discrete, pin-ended strips inclined in the direction of the tension field (Sabelli and Bruneau 2007) using 2-node truss elements (ABAQUS element T3D2). It was found that 12 and 10 pin-ended strips, shown in Figs. 8 and 9, were adequate to represent the infill plates of SW-A-H and SW-B-H, respectively. Gravity load was not applied in the testing or in the models.

As for initial out-of-straightness, according to measurements performed before testing, maximum and minimum out-of-straightness of the infill plate is 9.80mm and -6.33mm in SW-A-H and 22.90 mm and −22.01 mm in SW-B-H, respectively. However, this initial imperfection was neglected in the strip models of the TSPSW specimens. It is also demonstrated that overall load-displacement behavior is largely independent of initial deformed configuration of infill plate (Driver *et al.* 1998).

An inclination angle of 45° was assumed for the strips of the infill plate in Specimen SW-A-H, which is typical for the case of rigid beams and columns. Furthermore, the inclination can also be computed through consideration of Eq. (1) (Timler and Kulak 1983), resulting in 44.3°. For the orientation of the strips in SW-B-H, the incomplete diagonal tension field theory was considered (Thorburn *et al.* 1983), where the inclination angle of the tension field, α, is equal to *tan^{-1}(L/h) / 2*, resulting in 28.2° with respect to vertical. In strip model of SW-B-H, an inclination angle of 28° was used for the strips. Such small differences in the inclination angles have been shown to have an insignificant impact on the response (Driver *et al.* 1998).
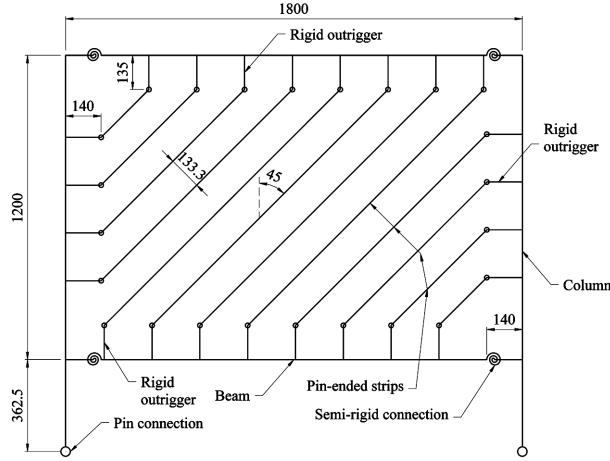
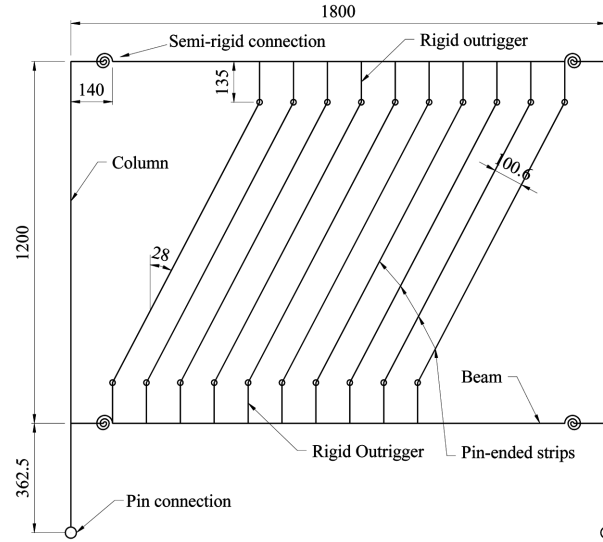Fig. 8 Strip model of specimen SW-A-H (Dimensions in mm)

Fig. 9 Strip model of specimen SW-B-H (Dimensions in mm)

$$tan^4\alpha \;=\; \frac{1 \times \dfrac{t_w L}{2 A_c}}{1 + t_w h\left(\dfrac{1}{A_b} + \dfrac{h^3}{360 I_c L}\right)} \tag{1}$$

α : Inclination angle of a strip
t_w : Thickness of the infill plate
L : Width of the SPSW (between column centerlines)
A_c: Section area of the column

h : Height of the SPSW (between beam centerlines)
A_b: Section area of the beam
I_c : Inertia moment of the column

Since the infill plate was connected to fish plates via self-drilling screws, each strip used for representing the infill plate should have screw connections at each end. For the sake of simplification, the effect of the screw connection on the behavior of strips was not included in the models of the TSPSW specimens. Thus, larger elongation of the strips due to bearing deformations at the ends, and in turn, larger initial stiffness than those obtained experimentally would be expected from the model. Rigid outriggers whose length were half of the section depths of the boundary frame members were utilized to account for the eccentricity between the infill plate edges and centerlines of the boundary frame members. Tension test results for yield stress and elastic modulus from the material test data for the infill plates described above were used for the material properties of the strip elements. The yield stress and elastic modulus of the boundary frame members was taken to be 275 MPa and 210000 MPa, respectively in the absence of coupon test results.

Since the behavior of the boundary frame is governed by the moment-rotation characteristics of the beam-to-column connections rather than the contribution of the relatively rigid beams and columns, the moment-rotation relationship for the header plate connection is needed. For modeling of the nonlinear behavior of header plate beam-to-column connections, the four parameter nonlinear representation of the moment-rotation curve expressed by the Eq. (2), was employed (Goldberg and Richard 1963, Abbott and Richard 1975)

$$ M = \frac{(K_\varphi - K_{\varphi,p}) \times \varphi}{\left(1 + \left|\frac{(K_\varphi - K_{\varphi,p}) \times \varphi}{M_o}\right|^n\right)^{1/n}} + K_{\varphi,p} \times \varphi \tag{2} $$

where K_φ, $K_{\varphi,p}$, M_o, M, n and φ are the initial and plastic stiffnesses, reference bending moment, computed bending moment, shape factor, and connection rotation, respectively. To apply Eq. (2) and develop the moment-rotation curve of a beam-to-column joint, the initial and plastic stiffnesses and the reference bending moment of the connection must be calculated. In addition, a reasonable range of rotation values should be used. Here, the initial stiffness, K_φ and reference bending moment, M_o, were initially obtained based on the provisions of Eurocode 3 (EC3) (European Convention for Constructional Steelwork 2004). In determining these parameters, the mean values of elastic modulus, yield and ultimate stresses for the header plates given in Table 2 were used. No reduction effect in Eq. (2) due to axial force was considered since it would be conservative to assume that this reduction is negligible (Berman and Bruneau, 2008).

For header plate connections, EC3 includes the following contributions to connection strength and stiffness: shear deformation of the column web, column web deformation in tension and compression, deformation of the header plate bolts in tension, bending deformations of the column flange, header plate deformations in bending and beam web deformations in tension. Considering these factors, M_o and K_φ were calculated to be 18.12 kNm and 7598 kNm/rad, respectively, where the reference moment was taken as the plastic moment capacity of the connection. It was assumed that the connection rotates about a point above the lower bolt row, thus the contribution of the lower bolt row to K_φ is neglected. The parameters $K_{\varphi,p}$ and n were found by calibrating the bare frame model with the test results for BF-H. The resulting values of $K_{\varphi,p}$ and n were found to be 531.86 kNm/rad, which corresponds to 7% of K_j,

and 1.7, respectively. These properties were then used in subsequent analyses of the strip models. The connection model parameters were calibrated over connection rotations from 0.00 rad to 0.026 rad. The resulting moment-rotation curve is given in Fig. 10 and was used as the input properties for the connection element in ABAQUS which used connector element CONN3D2. As shown in the figure, it was assumed that moment capacity of the connection was achieved at a rotation of 0.026rad, after which the moment-rotation curve was assumed to be flat.

The connection model, which incorporated the post-yield stiffness of the header plate connections and beam web material, that was observed in the quasi-static testing was included the pushover analyses of Specimens SW-A-H and SW-B-H. This enables the response of the infill plates and boundary frame to be separated. The pushover curves of the bare frame model and the strip models representing the TSPSW specimens are shown in Fig. 11. The ultimate strengths of the TSPSW
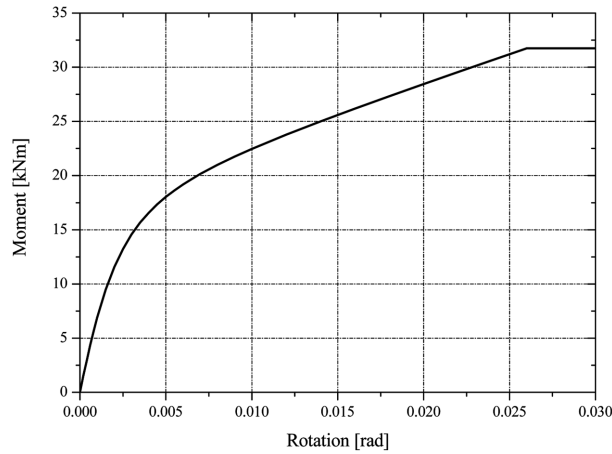
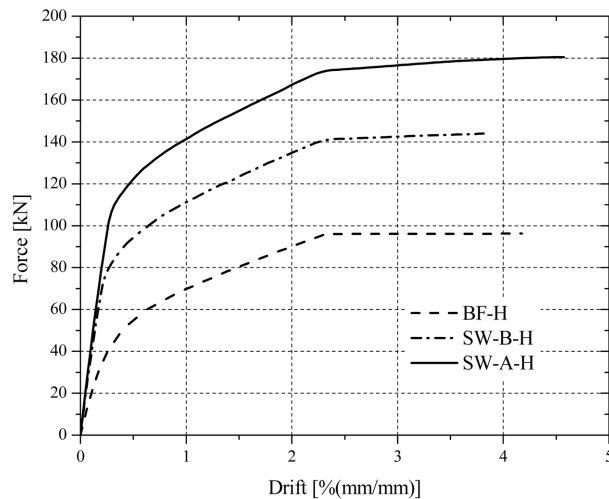Fig. 10 Moment-rotation curve for beam-to-column joint

Fig. 11 Pushover curves of the specimens

specimens were estimated to be 182 kN and 144 kN for SW-A-H and SW-B-H, respectively with no consideration of bearing deformations at screw connections.

5. Experimental results

The loading protocol of ATC 24 (Applied Technology Council 1992) which is recommended by Applied Technology Council (ATC) was followed. Table 3 shows the displacement history for each specimen. Below, experimental results are described using observations made during the tests and interpretation of the experimental data.

A total of twelve displacement transducers were used to measure deformations and typical arrangement of those was made as shown in Fig. 12 for all specimens. Drifts are calculated using TTE, TTW for top displacements and TNC4 for bottom displacements.

5.1. Specimen BF-H

The cyclic response of the Specimen BF-H is characterized by the stable hysteretic behavior as shown in Fig. 13, where the pushover curve from the analysis of the bare frame has been superimposed.

Specimen BF-H behaved elastically up to a drift of 0.57%. The initial stiffness of the frame was found to be approximately 16.036 kN/mm. When cracks in the paint were observed on the header plates in the beam-to-column connections indicating the onset of yielding, this drift was taken to be the yield drift, after which the hysteresis loops begin to open noticeably. After three cycles at this drift level the applied load was 81.0 kN. The maximum base shear was 97.6 kN and occurred at $+5\delta_y$ (3.52% drift) of Cycle 28, where δ_y is the yield displacement of the specimen. After the peak base shear strength degradation began slowly. At the end of the excursions of Cycle 32 at $\pm7\delta_y$, the ratio of the base shear to the maximum base shear was 0.80. The second excursion to $-7\delta_y$ caused fractures near the welded connection between header plate and beam web to propagate substantially, as shown in Fig. 14 and Fig. 15, respectively. This caused the resistance of the frame to degrade to 50% of the maximum base shear achieved and the test was terminated at this point.

5.2. Specimen SW-A-H

Specimen SW-A-H exhibited the cyclic response shown in Fig. 16. The specimen behaved elastically during the first 9 cycles of testing. After this point, some insignificant nonlinear behavior was observed. This nonlinearity occurred prior to yielding of the infill plate and is attributed to bearing of the infill plate behind the screws and also the initial out-of-straightness and local buckling of the infill plate. At 0.56% drift and a base shear of 107 kN during the first half of Cycle 19 the nonlinear behavior became significant and this was denoted the yield drift.

During cycles at $\pm3\delta_y$ (1.58% drift) plastic folds in the corners of the web plate and residual web plate buckling at zero drift became more evident. At $-5\delta_y$, a small infill plate tear of approximately 4.00 mm in length was observed in upper north corner, yet there was no degradation in the strength of the shear wall. During the cycles at the final displacement step, $\pm7\delta_y$, which corresponds to 3.67% drift, large residual buckles became visible at zero drift, which indicated that the plate had undergone significant plastic elongation. The specimen was subjected to one cycle at this displacement step because the net section failure of the infill plate along the upper edge occurred at the end of the first excursion as shown

Table 3 Cyclic displacement histories

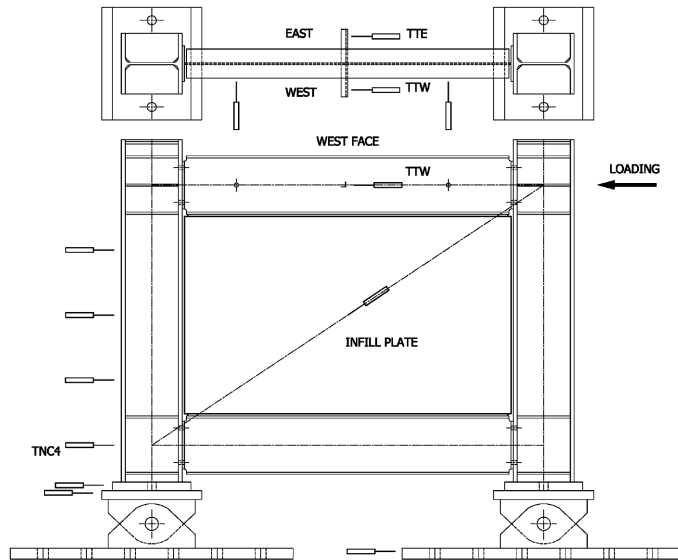| Disp. Step	Number of Cycles	Cumulative No. of Cycles	Relative Disp. Ratio to d_y (Δ/δ_y)	Relative Disp. [mm]	Drift (%)
BF-H					
1	3	3	0.17	1.41	0.12
2	3	6	0.34	2.80	0.23
3	3	9	0.51	4.18	0.35
4	3	12	0.67	5.52	0.46
5	3	15	0.83	6.86	0.57
6	3	18	1	8.22	0.68
7	3	21	2	16.65	1.38
8	3	24	3	25.17	2.10
9	2	26	4	33.71	2.81
10	2	28	5	42.19	3.52
11	2	30	6	50.71	4.23
12	2	32	7	59.68	4.97
SW-A-H					
1	3	3	0.14	0.92	0.08
2	3	6	0.27	1.82	0.15
3	3	9	0.40	2.72	0.23
4	3	12	0.54	3.64	0.30
5	3	15	0.74	4.98	0.42
6	3	18	0.87	5.89	0.49
7	3	21	1	6.77	0.56
8	3	24	2	12.84	1.07
9	3	27	3	19.00	1.58
10	2	29	4	25.38	2.12
11	2	31	5	31.39	2.62
12	2	33	6	37.71	3.14
13	1	34	7	44.00	3.67
SW-B-H					
1	3	3	0.13	0.78	0.07
2	3	6	0.25	1.52	0.13
3	3	9	0.37	2.26	0.19
4	3	12	0.47	2.89	0.24
5	3	15	0.58	3.56	0.30
6	3	18	0.69	4.24	0.35
7	3	21	0.79	4.88	0.41
8	3	24	0.89	5.53	0.46
9	3	27	1	6.18	0.52
10	3	30	2	12.07	1.01
11	3	33	3	17.95	1.50
12	2	35	4	23.74	1.98
13	2	37	5	30.45	2.54
14	1/2	37.5	6	37.65	3.14

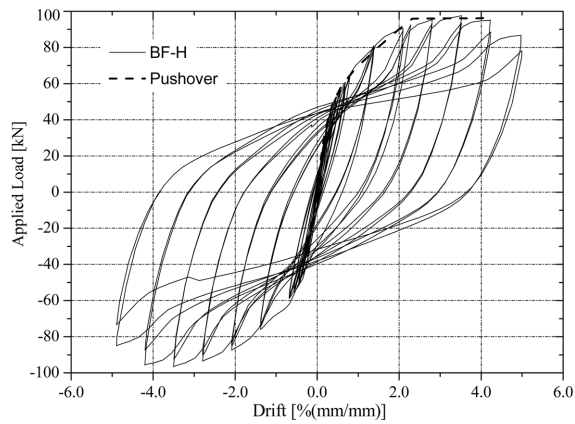Fig. 12 Arrangement of displacement transducers for all specimens
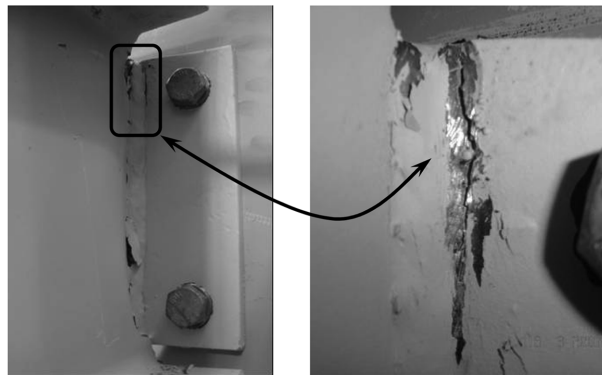

Fig. 13 Hytereses loops of specimen BF-H

Fig. 14 Header plate fracture (cycle 31 and top disp. of 81.81 mm)
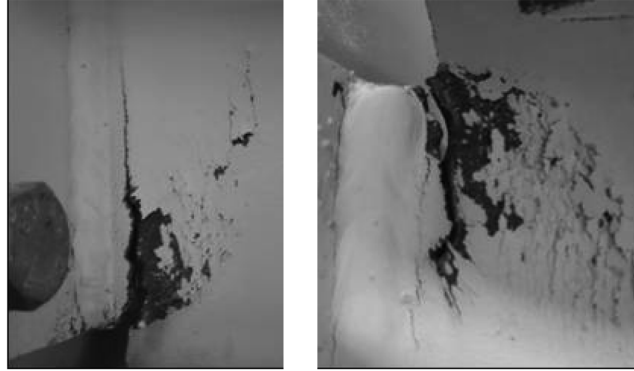
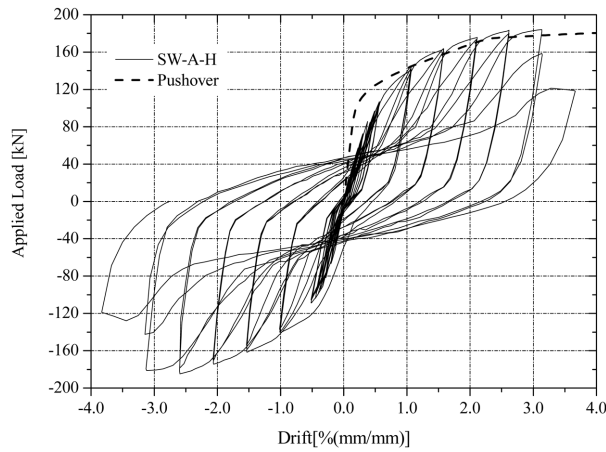Fig. 15 Beam web fracture (cycle 32 and top disp. of 81.81 mm)

Fig. 16 Hysteresis loops of specimen SW-A-H

in Fig. 17. The maximum base shear achieved during the final cycle of loading was 118 kN, 35.5% less than the maximum base shear. There were no indications of fractures in the beam-to-column connections at the end of the test.

5.3. Specimen SW-B-H

Specimen SW-B-H exhibited the cyclic response shown in Fig. 18. Some nonlinearity in the response was again evident prior to infill plate yielding that can be attributed to bearing of the screw connections, initial buckling and out-of-straightness of the infill plate. This nonlinearity was minor though deemed to be relatively insignificant.

At 0.52% drift and a load of 94 kN during the first half of Cycle 25 more significant nonlinear response was observed. Tension field orientation angle of less than 40° from vertical was also observed at this stage as demonstrated by the infill plate buckling waves shown in Fig. 19(a). The base shear was 127 kN and was achieved during the first half of Cycle 31 at 1.50% drift. During Cycle 34 at 1.98% drift, a 45 mm long net section fracture of the infill plate was observed at upper north corner. This
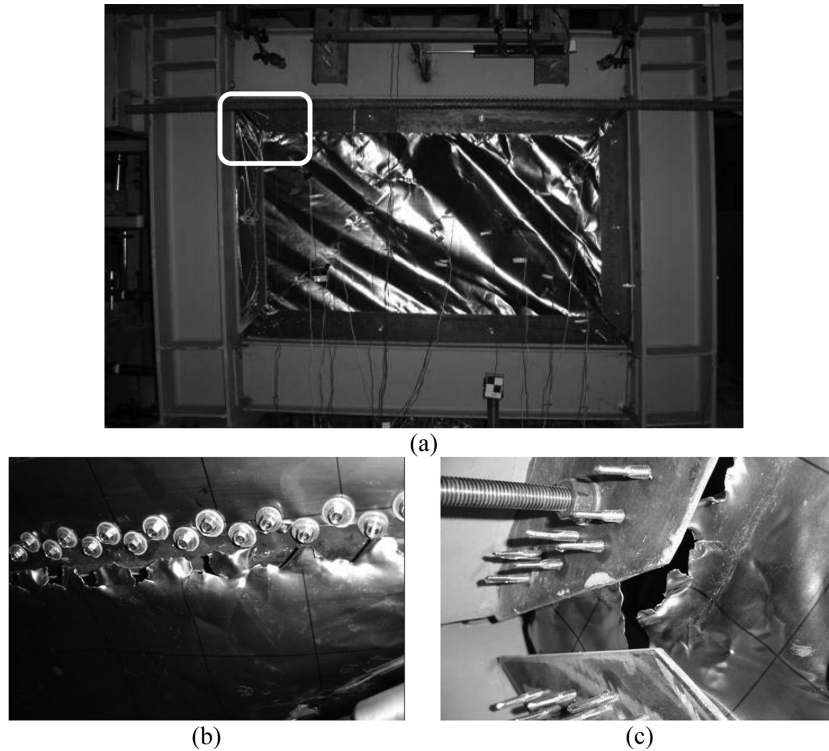
(a)

(b)

(c)

Fig. 17 (a) Buckling of infill plate, (b) and (c) Net section failure in north upper corner (Cycle 34 and top disp. of ±58.80 mm)
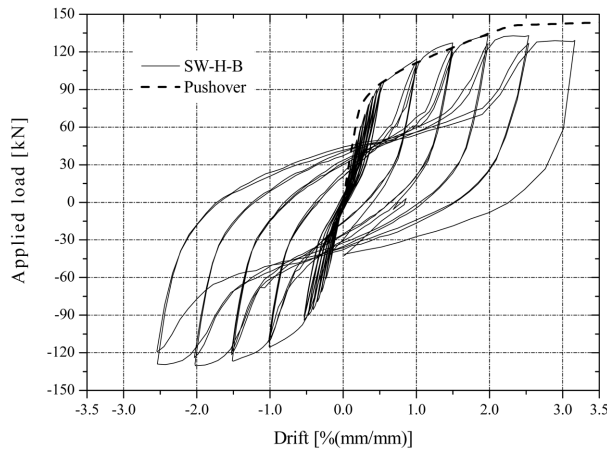

Fig. 18 Hysteresis loops of specimen SW-B-H

fracture occurred at a load of 133 kN. During the second excursion of the cycles to $-4\delta_y$, approximately 40mm long fractures at the net sections of the infill plates in the upper south and lower north corners were observed. However, this damage resulted in only a 5% decrease in the peak base shear during the
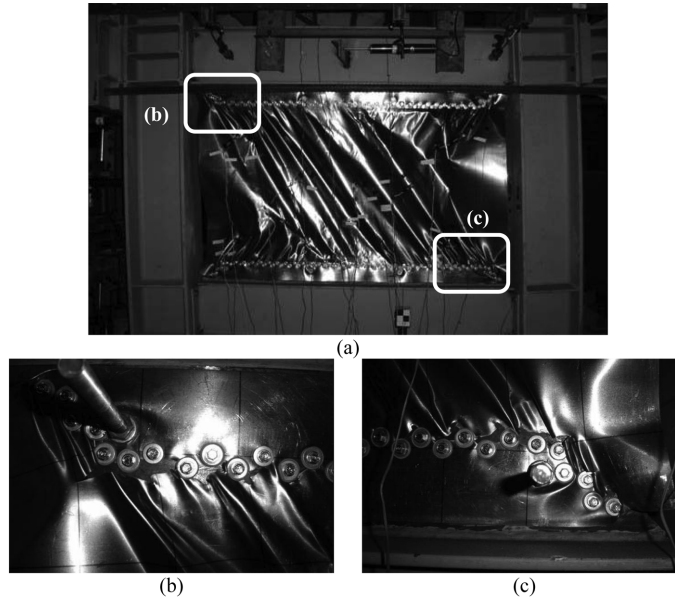
Fig. 19 (a) Buckling of infill plates and infill plate fracture in; (b) upper north corner, (c) lower south corner (Cycle 38 and top disp. of +50.61 mm)

cycles at $\pm 4\delta_y$. During the first half of Cycle 37, the fractures in the lower south and upper north corners of the infill plate grew to approximately 75 mm and 100 mm long, respectively. Again, despite these large fractures no significant strength degradation was observed and the base shear for the cycles at $\pm 5\delta_y$ was 127 kN. The test was terminated after the first half cycle at $\pm 6\delta_y$, to prevent test devices from damage in the event of rapid failure of the infill plate. During this final displacement step, infill plate tears in the corners grew to what is shown in Fig. 19(b) and (c). The fracture in upper north corner was 185 mm long while that in lower south corner was 150 mm long. A maximum base shear during the final half cycle of loading of 128kN was achieved at $+6\delta_y$.

6. Comparison of the results and discussion

The strength of the specimens may be compared by examining the experimental results at specified drift levels. Table 4 lists the strength of the TSPSW specimens at key drift levels normalized by the strength of Specimen BF-H at those same drift levels. Table 5 shows the maximum strength of the all three specimens and the maximum strength of the TSPSW Specimens relative to Specimen BF-H. From Table 4, it is apparent that the infill plates in both Specimen SW-A-H and Specimen SW-B-H contribute significantly to the strength of the walls until 3% drift, which corresponds to approximately $4\delta_y$ and $6\delta_y$ for Specimen BF-H and for both TSPSW specimens, respectively. Note that, Specimen BF-H did not suffer strength degradation until the final loading stages and in fact continued to gain strength until then. Thus, the maximum ratio of TSPSW strength to bare frame strength at specific drift levels, i.e., the maximum of the ratios given in Table 4, is not the same as the ratio of the maximum strengths given in Table 5. While greater strength is obtained with Specimen SW-A-H, Tables 4 and 5 demonstrate that TSPSWs with infill plates connected only to the beams do add considerable strength

Table 4 Ratio of required load at various drift levels

Drift [%]	SW-A-H / BF-H	SW-B-H / BF-H
0.50	1.80	1.71
0.75	1.91	1.65
1.00	1.95	1.64
1.50	1.94	1.54
2.00	1.94	1.49
2.50	1.95	1.42
3.00	1.92	1.36

Table 5 Ultimate load capacity

Specimen	Ultimate Load Capacity [kN]	Ratio Definition	Ratio
BF-H	97.60	BF-H / BF-H	1.00
SW-A-H	184.10	SW-A-H / BF-H	1.89
SW-B-H	133.10	SW-B-H / BF-H	1.36

and may be a viable lateral load resisting system.

The relative stiffnesses of the specimens are also evaluated to investigate the benefits of the infill plates and impact of the extent of the infill plate-to-boundary frame connection. To obtain the initial stiffness of the specimens, the first few points of the envelope response, for both loading to the north and south are considered. The ratios of the initial stiffness of Specimens SW-A-H and SW-B-H to that of Specimen BF-H are tabulated in Table 6. The values in Table 6, which were calculated as the average of the values from loading to the north and south, indicate that the infill plates add considerable stiffness to the bare frame, with a 73% increase in initial stiffness for Specimen SW-A-H and a 41% increase for Specimen SW-B-H. Again, the significant contribution to initial stiffness for both specimens indicates that connecting the infill plate to only the beams of the boundary frame is a viable option.

As can be seen in Figs. 16 and 18 which show the hysteretic behavior of Specimens SW-A-H and SW-B-H, respectively, both specimens exhibit slip-stick behavior at small displacement levels, which is demonstrated in Fig. 20. For Specimen SW-A-H the behavior is more pronounced, i.e., the slip portion of the deformation response due to the bearing deformations at the screw holes is larger than that of Specimen SW-B-H. This difference in behavior can be partially attributed to the difference in infill plate attachment. In Specimen SW-B-H, where the infill plate is connected to only the boundary frame beams, the tension field does not develop over the entire beam length, so in each cycle there are some screws which do not slip and holes which are not subjected to bearing in both directions. In contrast, the Specimen SW-A-H develops tension field action over the entire infill plate and all screws slip and all holes bear in the two orthogonal directions of tension field formation for both directions of loading. Therefore, more bearing deformations would be expected to be present in the hysteretic behavior of

Table 6 The ratio of total initial stiffness

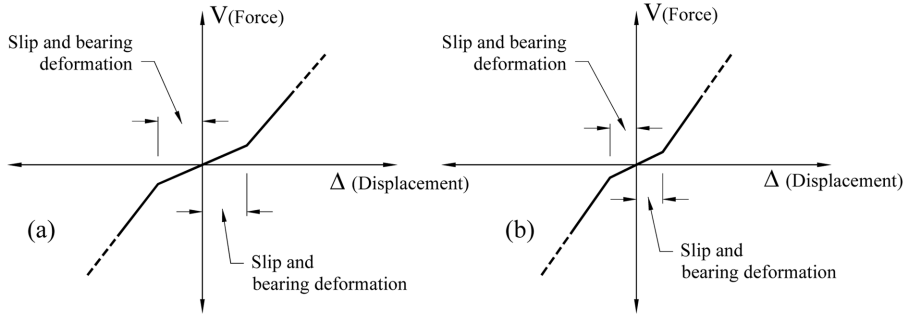| Specimen	Total initial stiffness [kN/mm]	Ratio definition	Ratio
BF-H	15.784	BF-H / BF-H	1.00
SW-A-H	27.260	SW-A-H / BF-H	1.73
SW-B-H	22.288	SW-B-H / BF-H	1.41

Fig. 20 Typical response of a tension field with the consideration of bearing deformations; (a) in SW-A-H and (b) in SW-B-H
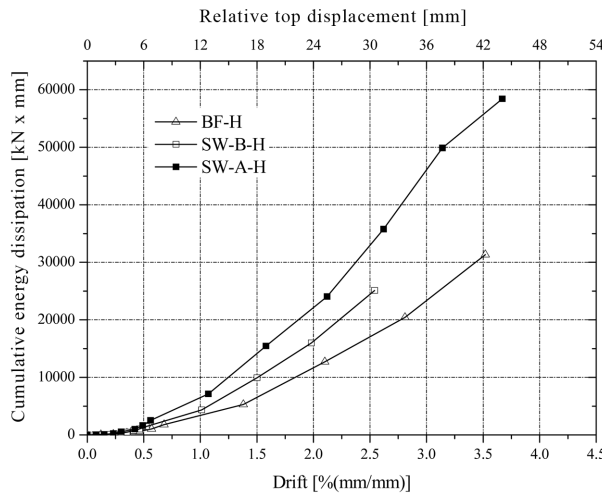

Fig. 21 Comparison of cumulative energy dissipation

Specimen SW-A-H.

Energy dissipation is an important consideration in seismic design. The cumulative energy dissipation of the specimens is plotted versus the drift in Fig. 21. The energy dissipation was calculated using all cycles of each displacement increment and is the area enclosed by the load displacement curve. As shown, Specimen BF-H dissipates energy at a low rate compared to TSPSW specimens. Energy dissipation for Specimen BF-H begins at the onset of header plate yielding at the beam web-to-header plate connection and then increases slightly as yielding progresses to the regions in beam web. In the TSPSW specimens energy dissipation begins with bearing of the plate at infill plate-to-fish plate connections and increases with infill plate yielding and header plate connection yielding.

At 2.5% drift, the cumulative energy dissipation of Specimens SW-A-H and SW-B-H was approximately 2.00 and 1.5 times that of Specimen BF-H, respectively. Again, while the performance of Specimen SW-A-H was superior to that of Specimen SW-B-H, the performance of Specimen SW-B-H relative to Specimen BF-H indicates significant benefit from the infill plates. Adding the infill plate and connecting it to only the beams might therefore be a viable alternative, especially when retrofitting

SW-A-H
Cycle 32 and top disp. of +50.39mm

SW-B-H
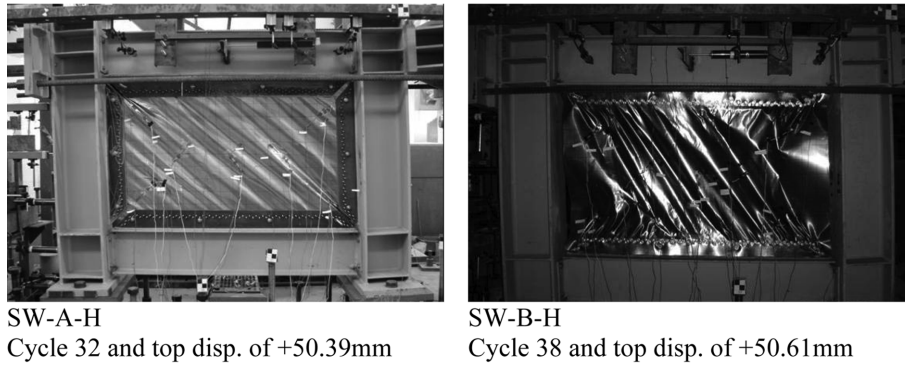Cycle 38 and top disp. of +50.61mm

Fig. 22 Tension field orientations in the infill plates

frames having columns with possibly insufficient flexural strength and stiffness.

It is necessary to obtain the orientation of the buckling waves or tension field for development of the simplified strip model for TSPSW systems. The difference in the orientation of the tension fields at almost equal displacement levels for Specimens SW-A-H and SW-B-H is clearly shown in Fig. 22. Based on observations, the angle of the tension field with respect to the vertical in the infill plate of SW-B-H is between 30° and 35°, while for Specimen SW-A-H it is approximately 45°. Using a computed angle that is less than the observed angle would result in a slightly conservative estimate of the strength of the TSPSW using conventional methods. Therefore, the incomplete tension field approach seems to be useful for computing the orientation angle.

The TSPSW specimens utilizing screwed infill-to-fish plate connections were found to be reasonably ductile. Failures inevitably resulted from fractures in the net sections of the infill plates at the screw connections. Despite these fractures, which appeared first at $-5\delta_y$ for Specimen SW-A-H and at $-4\delta_y$ for Specimen SW-B-H, there was not significant loss of strength until cycles at $6\delta_y$ for both specimens.

7. Conclusions

Two TSPSWs were tested under quasi-static loading and a bare frame was also tested to quantify the beam-to-column response. While one TSPSW was composed of an infill plate connected to the boundary frame on all four edges, other one had an infill plate that was connected only to the beams of the boundary frame.

The experimental results demonstrate that the stiffness and the ultimate strength of steel frames with semi-rigid beam-to-column connections can be increased by adding thin infill plates provided that the infill plate-to-boundary frame connection is designed properly. The contribution of the infill plate connected only to the beams of the boundary frame was found to be significant in terms of energy dissipation, initial stiffness and lateral strength. Hence, TSPSWs with infill plates attached only to the beams should be useful for retrofitting and strengthening steel frames that have inadequate stiffness and strength with reduced labor and material savings due to absence of the connections between columns and infill plate edges. The incomplete diagonal tension field approach was found to be suitable for computing the orientation angle in TSPSWs with infill plates connected only to the beams. The

adequacy of strip models using calculated values for the tension field orientation angle in predicting the ultimate strength of TSPSWs designed using self-drilling screws for the infill plate connections was found to be acceptable through comparison with the experimental results. However, further research is needed on TSPSWs having infill plates with no connection to the columns and screwed infill plate-to-fish plate connections to develop models that consider the bearing deformation response revealed in the test results.

Acknowledgements

References

Abbott, B.J. and Richard, R.M. (1975), "Versatile elastic-plastic stress-strain formula", *J. Eng. Mech. Div.*, **101**(4), 511-515.

Alinia, M.M. and Dastfan, M. (2006), "Behavior of thin steel plate shear walls regarding frame members", *J. Constr. Steel. Res.*, **62**(7), 730-738.

Applied Technology Council (ATC), (1992), *ATC-24 Guidelines for Cyclic Seismic Testing of Components of Steel Structures*, California.

Berman, J. and Bruneau, M. (2003), "Plastic analysis and design of steel plate shear walls", *J. Struct. Eng.*, **129**(11), 1448-1456.

Berman, J. and Bruneau, M. (2005), "Experimental investigation of light-gauge steel plate shear walls", *J. Struct. Eng.*, **131**(2), 259-267.

Berman, J. and Bruneau, M. (2008), "Capacity design of vertical boundary elements in steel plate shear walls", *AISC Eng. J.*, **45**(1), 57-71.

Bruneau, M. and Bhagwagar, T. (2002), "Seismic retrofit of flexible steel frames using thin infill panels", *Eng. Struct.*, **24**(4), 443-453.

Caccese, V., Elgaaly, M. and Chen, R. (1993), "Experimental study of thin steel-plate shear walls under cyclic loading", *J. Struct. Eng.*, **119**(2), 0573-0587.

Choi, I.R. and Park, H.G. (2009), "Steel plate shear walls with various infill plate designs", *J. Struct. Eng.*, **135**(7), 785-796.

Driver, R.G., Kulak, G.L., Elwi, A.E. and Kennedy, D.J.L. (1998), "FE and simplified models of steel plate shear wall", *J. of Struct. Eng.*, **124**(2), 0121-0130.

Driver, R.G., Kulak, G.L., Kennedy, D.J.L. and Elwi, A.E. (1998), "Cyclic test of four-story steel plate shear wall", *J. of Struct. Eng.*, **124**(2), 0112-0120.

Elgaaly, M. and Liu, Y. (1997), "Analysis of thin-steel-plate shear walls", *J. Struct. Eng.* **123**(11), 1487-1496.

European Convention for Constructional Steelwork (ECCS), *Eurocode 3, Design of Steel Structures*, CEN, Brussels.

Ghosh, S., Adam, F. and Das, A. (2009), "Design of steel plate shear walls considering inelastic drift demand", *J. Constr. Steel Res.*, **65**(7), 1431-1437.

Goldberg, J.E. and Richard, R.M. (1963), "Analysis of nonlinear structures", *J. Struct. Div.*, **89**(4), 333-351.

Hibbit, Karlsson, Sorenson, Inc., (HKS), *ABAQUS/Standard Theory Manual*, Student Version 6.4.

Lubell, A.S., Prion, H.GL., Ventura, C.E. and Rezai, M. (2000), "Unstiffened steel plate shear wall performance under cyclic loading", *J. Struct. Eng.*, **126**(4), 0453-0460.

Memarzadeh, P., Azhari M. and Saadatpour, M.M. (2010), "A parametric study on buckling loads and tension field stress patterns of steel plate shear walls concerning buckling modes", *Steel. Comp. Struct.*, **10**(1), 87-108.

Sabelli, R. and Bruneau, M. (2007), *Design Guide 20 Steel Plate Shear Walls*, American Institute of Steel Construction.

Sabouri-Ghomi, S., Ventura, C.E. and Kharrazi, M.H.K. (2005), "Shear analysis and design of ductile steel plate walls", *J. of Struct. Eng.*, **131**(6), 878-889.

Thorburn, L.J., Kulak, G.L and Montgomery, C.J. (1983), *Analysis of Steel Plate Shear Walls*, Structural Engineering Report No 107, Edmonton (AB), Dep. Civil Eng., University of Alberta.

Timler, P.A and Kulak, G.L. (1983), *Experimental Study of Steel Plate Shear Walls*, Structural Engineering Report No 114, Edmonton (AB), Dep. Civil Eng., University of Alberta.

Tromposch, E.W. and Kulak, G.L. (1987), *Cyclic and Static Behavior of Thin Panel Steel Plate Shear Walls*, Structural Engineering Report No 145, Edmonton (AB), Dep. Civil Eng., University of Alberta.

Vatansever, C. (2008), *Cyclic Behavior of Thin Steel Plate Shear Walls with Semi-Rigid Beam-to-Column Connections*, PhD. Thesis, Istanbul Technical University, Institute of Science.

Vian, D., Bruneau, M. and Purba, R. (2009), "Special perforated steel plate shear walls with reduced beam section anchor beams II: Analysis and design recommendations", *J. Struct. Eng.*, **135**(3), 221-228.

Xue, M. and Lu, L.W. (1994), "Monotonic and cyclic behavior of infilled steel shear panels", *Proceedings of 17th Czech and Slovak Int. Conf. on Steel Struct. and Bridges*, Bratislava, Slovakia.

CC